Physical model of voltage sensing in sodium channels based on the sliding helix complex

C. C. Chancey[1,*] and S. A. George[2]
[1]*Department of Physics and Chemistry, Purdue University Calumet, Hammond, Indiana 46323-2094*
[2]*Department of Biology and Neuroscience Program, Amherst College, Amherst, Massachusetts 01002-5000*
(Received 19 June 1995)

We have modeled voltage sensing in the sodium channel by evaluating forces on the $S4$ α-helix portion of the channel molecule, which we assume moves outward during activation. The interaction between the $S4$ α-helix segment and its environment was modeled by (i) nearest-neighbor Coulombic forces, (ii) the electric force due to an external electric field, and (iii) static mechanical and electrostatic forces. These terms collectively describe a depolarization-dependent effective potential within which the $S4$ segment moves. Thermal transitions between center-of-mass energy states of the segment were modeled starting from the Boltzmann distribution, and the time evolution of the segment's position relative to the membrane was simulated. Combining the histories of four such processes models the activation history of the channel molecule. The model simulation is in good qualitative agreement with batrachotoxin-modified single channel open and closed dwell time distributions and with such a channel's open probability as a function of depolarization. The model also qualitatively agrees with site-specific mutagenesis experiments, which show the different effects of eliminating positive charges on the cytoplasmic and extracellular ends of the $S4$ segment.

PACS number(s): 87.10.+e, 87.15.By, 87.22.Bt

I. INTRODUCTION

Ion channels are macromolecular pores in cell membranes that open and close to regulate the diffusion of ions across the membrane [1]. In the cells of excitable tissues, such as those of nerve and muscle, ion channels are the molecular structures that underlie electrical signal transmission [2]. Ion channels that open and close in response to variations in transmembrane voltage differences have long been known to be the subcellular unit involved in production of the action potential in neurons [3].

These voltage-sensitive ion channels fluctuate between open and closed states on a millisecond time scale. Statistical characteristics of these fluctuations, such as the fraction of time spent in the open state and the distribution of open and closed times, are functions of membrane potential and temperature. Several existing statistical analyses provide good fits to some of the observed channel statistics [1]. While these models are valuable in uncovering stochastic processes that underlie channel activity, none of the models is based on a physical framework involving well-defined forces acting on known structures, such as those thought to be involved in voltage sensing and channel activation. In this paper we explore a simple physical model that incorporates Coulombic and other forces on the sodium channel's presumed voltage sensor, the $S4$ segment of the channel molecule. We limit our analysis to modeling activation and do not deal with the separate activation process found in many types of channels. Our goal in this research is to investigate whether such a model is consistent with the available data on channel activation.

Several lines of evidence suggest that the voltage sensor is the $S4$ segment, an α-helical transmembrane segment containing four to eight positively charged amino acids that are highly conserved in many voltage-sensitive channels. The configuration of this segment relative to its immediate environment is, however, a matter for speculation. Specifically, the orientation of the $S4$ segment within the cell membrane, the segment's interaction with other transmembrane segments, and its detailed mechanical connection to pore opening can only be conjectured. Several researchers have suggested that a screw translation of the α helix, driven by membrane depolarization, is tied directly to the movement of the gating charges [4–6]. This ''sliding helix'' model, though simple and conjectural, does provide a plausible starting point from which to consider one possible mechanism of voltage-gated activation.

Our object in studying this model is to gain preliminary insight into whether the sliding helix picture is physically tenable. The analysis outlined in this paper makes several simplifying assumptions: (i) that all four $S4$ segments are identical, with each containing six positively charged arginine or lysine residues; (ii) that they operate independently; (iii) that the conformational change of the $S4$ segment is accomplished by a sliding translation that follows a left-handed helical path; (iv) that the channel pore is open if and only if at least three of the four homologous repeats in the sodium channel molecule are activated; (v) that activation may be modeled independently of inactivation; and (vi) that batrachotoxin-treated axons, although different in many respects from native axons, possess normal gating mechanisms, so that data from batrachotoxin-treated axons may be used for comparison with the results from the model.

In regard to the first assumption, a number of investigators have shown that individual $S4$ units are not identical [7–9]. The multiple time constants of gating currents [10] and the observed time constant of tail currents [11] have both been interpreted as evidence for coupling between gates [9], an observation that would moderate our second assumption. Our assumption that the $S4$ segment slides by way of a screw translation concentrates on center-of-mass (c.m.) mo-

*Author to whom correspondence should be addressed.

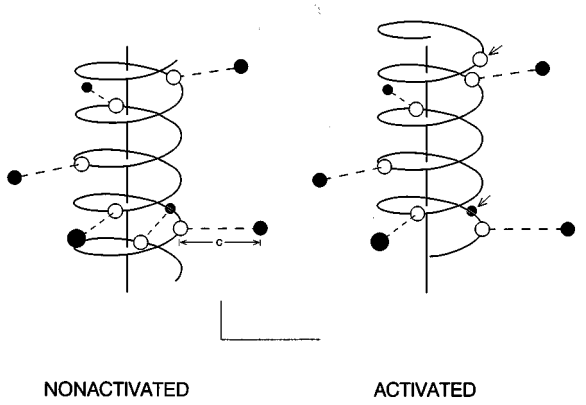

FIG. 1. Pictorial representation of activation in the sliding helix model. Open circles (○), positions of positive charges; filled circles (●), position of putative negative charges on adjacent segments of the channel molecule. Each positive charge and its nearest-neighbor charge are joined by a dashed line. (In calculating Coulombic potentials, the interaction of each positive charge with *all* negative charges were computed.) Vertical and horizontal scale marks indicate 5 Å, showing that the vertical scale has been compressed in this diagram. The minimum distance c between positive and negative charges is shown for one pair of charges; in this figure, $c=4.2$ Å. After the shift and rotation associated with activation, the outermost positive charge and innermost negative charge no loner have a near-neighbor opposite charge (arrows).

tion at the expense of other modes of the segment, such as torsional and compressional oscillations of the helix about the c.m. Ignoring these other modes can be expected to affect the model's closed-to-open transition rates—a point we address in Sec. VI. Finally, given recent estimates of gating charge movement [12,13], the assumption of the sliding helix model that a single elementary positive charge moves outward across the membrane during activation may not be accurate. While we recognize the limitations inherent in the above simplifications, we believe that the postulated helical-screw motion of the $S4$ segment is better studied within the simpler regime that these simplifications afford.

II. MODEL

The sliding helix concept of activation is illustrated in Fig. 1, showing the position of charged residues on the $S4$ α helix and on other transmembrane segments near the $S4$ helix. Positive charges in the helix are shown by open circles and putative negative charges on adjacent segments of the channel molecule by filled circles. During activation, the helix is assumed to move rigidly outward, with no changes in the distances between positively charged residues within the helix and no changes in the positions of the negative charges. With an assumed spacing of 3.6 amino acids per turn of the helix and a distance of 1.5 Å between the centers of residues measured along the axis of the helix, the positive charges will be 4.5 Å apart measured along the axis and will have an angular separation of 300°.

Moving in the electrostatic field created by the negatively charged residues, the α helix will have two stable locations: one (corresponding to the nonactivated state) entirely within the membrane and another (corresponding to the activated state) shifted outward and rotated by an amount needed to bring each positive charge into the position occupied by the one above it in the nonactivated state. Thus the outward shift during activation is 4.5 Å and the helix is rotated by $+300°$ or, equivalently, by $-60°$. The vertical line through the helix in Fig. 1 indicates the approximate thickness of the membrane in the region of the helix.

The kinematics of this center-of-mass motion by the α helix are determined by the effective potential within which the helix moves. In previous work [14], this potential was evaluated by considering the effects of four forces on the helix: (i) electrostatic attractions between the positively charged $S4$ residues and an equal number of postulated negatively charged residues assumed to be located in adjacent portions of the channel molecule along a helical path outside the $S4$ helix; (ii) the electric force on the helix due to the resting potential difference across the membrane; (iii) tensile and other forces on the helix, due to its position in the channel molecule, which act to counterbalance the Coulombic binding; and (iv) electric forces on the helix due to an external electric field, such as is applied during electrical stimulation or voltage clamping. The net result of the last three forces can be represented by an effective electrostatic force on the α helix, $6QE_{\text{eff}}$ where E_{eff} is an effective field representing the sum of all non-Coulombic forces.

The forces outlined above combine to define a potential energy function for the displacement of the $S4$ helix along an axis z normal to the membrane. Measuring displacement along this axis, this effective potential $U_{\text{tot}}(z)$ takes the form

$$U_{\text{tot}}(z)=[U_{\text{Coul}}(z)-U_{\text{Coul}}(z=0)]-6Q\vec{E}_{\text{eff}}\cdot\vec{z}, \qquad (1)$$

where $U_{\text{Coul}}(z)$ is the potential energy arising from the helix's Coulombic binding to nearest-neighbor residues; the constant term $-U_{\text{Coul}}(z=0)$ in $U_{\text{tot}}(z)$ is included to ensure that $U_{\text{tot}}(z=0)=0$, a calculational convenience; and $6QE_{\text{eff}}$ is an effective force that combines the effects of all other forces on the α helix expressed in terms of an effective electric field E_{eff}. Within $U_{\text{tot}}(z)$, the potential energy arising from the helix's Coulombic binding to nearest-neighbor residues is represented by $U_{\text{Coul}}(z)$, given by

$$U_{\text{Coul}}(z)=\sum_{p=0}^{5}\sum_{n=0}^{5}\frac{k_m Q}{d_{pn}(z)^2}. \qquad (2)$$

In this equation d_{pn} is the distance between a positive residue indexed by p and a negative residue specified by n and k_m is the electrostatic force constant appropriate to the residue-residue interaction. It is related to the permittivity ϵ_m by $k_m=1/4\pi\epsilon_m$, with $\epsilon_m=\epsilon_0\epsilon_r$, where ϵ_r is the permittivity (or dielectric constant) and $\epsilon_0=8.85\times10^{-12}$ F/m is the permittivity of free space. In the absence of detailed information about the composition of the spaces between adjacent transmembrane segments, ϵ_r was allowed to range between 5 and 20, values appropriate on the atomic level for peptides.

The positively charged residues in a right-handed $S4$ α helix shown in Fig. 1 can be described mathematically as lying along a *left-handed* helix of radius a and pitch b, and this representation is convenient to use in calculations. The rotation during activation will be $+60°$ along the left-handed helix. With the minimum separation distance between posi-

tive and negative residues denoted by c, the distance between positive residue p and negative residue n is given by

$$d_{pn}(z)=\left\{c^2+2a(a+c)\left[1-\cos\left(\frac{(p-n)\pi}{3}-\frac{z}{b}\right)\right]+b^2\left(\frac{(p-n)\pi}{3}-\frac{b}{z}\right)^2\right\}^{1/2}. \quad (3)$$

In deriving this expression, we have positioned the negative and positive residues, using circular cylindrical coordinates, as

$$(r_n,\theta_n,z_n)=(a+c,n\pi/3,-bn\pi/3) \quad (4)$$

and

$$(r_p,\theta_p,z_p)=\left(a,\frac{p\pi}{3}-\frac{z}{b},z-\frac{bp\pi}{3}\right), \quad (5)$$

where n and p index the positions of the negative and positive charges, respectively, with both indices running from 0 to 5. The z axis tracks the α helix's shift and thus enters the position coordinates of the positive residues [4]. We take $a=2.5$ Å as the radius of the α helix and $b=4.3$ Å/rad. This value is equal to 27 Å/2π, where 27 Å is the length of the left-handed helix over one complete turn of 2π rad. (In the sliding helix model, the six positively charged residues are separated by angles of 60° around this left-handed helix and thus cover only 300° along the helix, corresponding to an axial distance of 22.5 Å.) The minimum distance c between positive and negative charges was varied in initial calculations between 3 and 6 Å. The lower of these values was suggested by the sum of the van der Waals radii of nitrogen and oxygen [15] and the higher value by helix packing theory [16]. As will be seen in Sec. IV, only a subset of the 3–6 Å range of values of c is capable of modeling the behavior of sodium channels.

As described above, the effective field $E_{\rm eff}$ combines several distinct influences on the $S4$ segment. Specifically,

$$\vec{E}_{\rm eff}=\vec{E}_{\rm ext}+\vec{E}_{\rm rest}+\frac{\vec{F}_{\rm bal}}{6Q}, \quad (6)$$

where $E_{\rm ext}$ is any applied electric field across the membrane, $E_{\rm rest}$ is the field associated with the resting membrane potential difference, and $F_{\rm bal}$ is a constant balancing force representing the sum of all remaining forces on the helix, discussed in detail below. The membrane potential difference $\Delta V_{\rm memb}$ changes with $E_{\rm ext}$ according to

$$\Delta V_{\rm memb}=\Delta E_{\rm ext}d,$$

where d is the local thickness of the membrane in the region of the $S4$ segment. Thus, since $E_{\rm rest}$ and $F_{\rm bal}/6Q$ are both assumed to be constant, changes in the membrane potential difference are the direct result of changes in $E_{\rm eff}$.

$$\Delta V_{\rm memb}=\Delta E_{\rm eff}d.$$

For purposes of computation, it is sufficient and convenient to use $E_{\rm eff}$ as the independent variable measuring membrane depolarization. Specific values for the three components of $E_{\rm eff}$ will be discussed below.

In what follows, we (i) set the energy levels of the double-well potential by a harmonic oscillator approximation, (ii) develop a computational routine for describing how the α-helix partitions its time among these allowed energy levels; (iii) use this routine to simulate the pattern of opening and closing of the channel, from which channel statistics, and the voltage and temperature dependences of the statistics, are calculated; (iv) compare these results with data from single batrachotoxin-modified sodium channels in the squid giant axon as measured by Correa, Bezanilla, and Latorre [17], and use this comparison to introduce a time scale into the model; and (v) comment on the effects of site-specific mutagenesis experiments in which charged amino acids in the $S4$ segment are replaced by neutral amino acids.

III. PRELIMINARIES

Evaluation of $U_{\rm tot}(z)$ revealed a double-well potential with each well nearly parabolic below the barrier between the wells. Thus, in modeling the dynamics of the α helix within the effective potential given by Eq. (1), we made the simplifying assumption that energy levels within and above each potential well can be approximated by a spectrum of equally spaced energies. Using a harmonic fit for both wells, we determined an energy level spacing ($\hbar\omega_0$) of 0.44 meV [14]. The allowed energies were placed according to $N\hbar\omega_0$ ($N=0,1,2,\ldots$) starting from the deeper of the two potential wells and continuing above the potential barrier. The energy levels in the shallower well were assumed to be equal to the corresponding energies in the deeper potential well. This simple procedure, though a rough approximation, produces results that are relatively robust to changes in the densities of the energy levels.

Using Eq. (1), the potential energy $U_{\rm tot}(z)$ was calculated for values of minimum charge separation c ranging from 3 to 6 Å. Figure 2 shows examples of the double-well potentials $U_{\rm tot}(z)$ for a separation between positive and negative charges of 4.55 Å [Figs. 2(a)–2(f)] and for a range of effective fields in each case. To model the observed voltage dependence of activation, effective fields must be chosen so that depolarizations of 10–30 mV produce a substantial increase in activation. Such an increase corresponds to a shift in the graph $U_{\rm tot}(z)$ from an asymmetric double well with a deeper left-hand (nonactivated) well—as in Figs. 2(a) and 1(d)—to one with a deeper right-hand (activated) well—as in Figs. 2(c) and 2(f).

For the α helix in thermal equilibrium with its environment, the relative probability of its occupying a given oscillatory state of energy E is given by $e^{-E/kT}$, where k is Boltzmann's constant and T is the temperature in degrees kelvin. A program was written to simulate the time evolution of the α helix among the allowed energy states. In each time step of the program, the helix was allowed to jump to any of the energy levels, with the probability of reaching a given level weighted according to the Boltzmann factor. Three energy regimes are defined by this approach: (i) a nonactivated state, in which the helix is confined to the leftmost potential well;

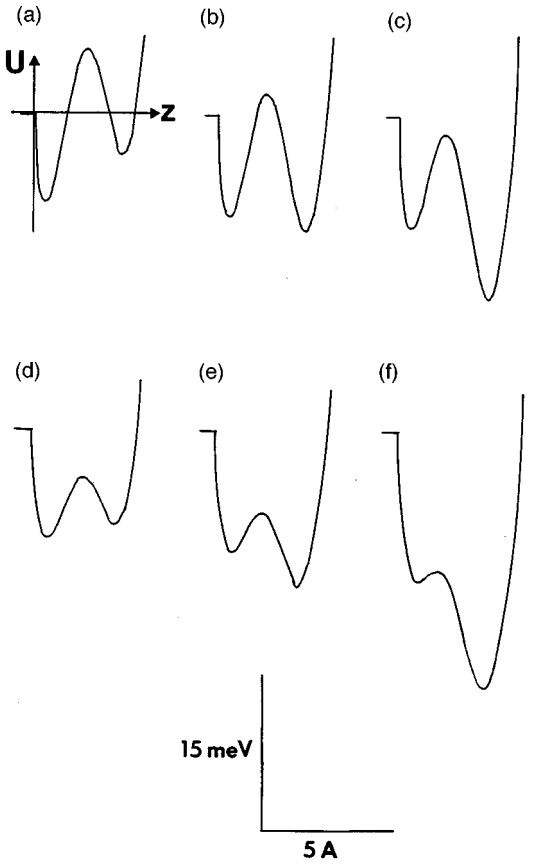

FIG. 2. Graphs of $U_{tot}(z)$, the effective potential for the $S4$ α helix, vs z, the position coordinate normal to the plane of the membrane. Upper 3 records: $U_{tot}(z)$ for minimum charge separation $c=4.55$ Å and for values of the effective electric field E_{eff} of (a) 0.0130 V/Å, (b) 0.137 V/Å, and (c) 0.150 V/Å. Higher values of E_{eff} correspond to greater depolarization of the membrane. The left-hand well in each double-well potential locates the nonactivated position of the helix; the right-hand well corresponds to the activated position. Activation is favored as depolarization increases (with increasing depth of the right-hand well). The dielectric constant is equal to 7. Effective fields were chosen to result in a probability of the channel being open of (a) and (d) 0.025, (b) and (e) 0.3, and (c) and (f) 0.6.

(ii) an activated state, in which the helix is within the right potential well; and (iii) a fluctuating state, in which the helix energy is above the top of the barrier between the wells and thus not bound in either activated or nonactivated positions. States in the fluctuating regime were permitted to have energies up to but not exceeding a ''cap'' of 100 meV (approximately $4kT$) as measured from the bottom of the deeper of the two wells. The cap is described more fully in Sec. VI, but it may be noted here that the value of 100 meV is far enough above the top of the barrier that the results were virtually unaffected by moderate variations in the cap.

In each cycle of the program, four independent calculations were done, each continuing for 500 time steps and each modeling one of the four $S4$ α helix voltage sensors associated with a single sodium channel molecule. The channel was considered to be open during a given time step if at least three of the four helices were in the activated state during the time step. The 500-step cycles were continued for several hundred iterations (with the beginning condition of a given cycle being set to the final condition of the previous one) to produce reliable sets of open and closed time intervals. One of these cycles is illustrated in Fig. 3. This figure simulates an $S4$ segment's time evolution over 500 cycles among the nonactivated, fluctuating, and activated regimes. In addition, four of these histories were used to construct the time sequence of channel opening and closing, as illustrated in the simulated patch clamp records at the bottom of Fig. 3.

IV. RESULTS

A. Constraints on charge separation

To model situations in which the channel can make spontaneous transitions between closed and open states, the depth of each well, measured from the top of the potential barrier between the wells, must be of the order of 25–50 meV (i.e., between kT and $2kT$ at biological temperatures), as in Figs. 2(a)–2(c). If the depth is less than 25 meV, as in Figs. 2(d)–2(f), spontaneous thermal fluctuations between nonactivated and activated states will occur so frequently that only a very narrow range of open and closed times are produced, rather than the observed range of approximately three orders of magnitude in open and closed times [17]. If the wells are much deeper than 50 meV, the helix becomes locked in either the nonactivated or the activated state for very long times, until the improbable occurrence of a jump to a high energy level above the barrier and a transition into the alternate well (data not shown).

The depth of the potential energy wells for the α helix depends on (i) the number of positive and negative charges on the helix and on surrounding segments, (ii) the separation c between positive and negative charges, and (iii) and local dielectric constant ϵ_r within the membrane. Figure 4 indicates how these variables affect the depth of the wells. For each of the six curves, the effective field was chosen to produce wells of equal depth and that depth is shown as a function of charge separation from 3 to 6 Å. Three pairs of curves are shown, for dielectric constants of 5, 10, and 20, and, for each dielectric constant, a curve calculated assuming six negative charges and one assuming five negative charges. (All of the curves assume six positive charges on the $S4$ α helix.) The requirement for well depths of approximately 25–50 meV limits the acceptable charge separation in the model to a small part of the 3–6 Å range. For example, $\epsilon_r=5$ and six negative charges (rightmost curve in Fig. 4) the range is 4.6–4.95 Å. When the minimum separation between positive and negative charges becomes greater than the distance between successive positive charges on the α helix, there is little variation in the Coulombic attraction between the helix and surrounding charges as the helix moves outward and therefore little variation in the potential energy of the helix.

B. Open probability and depolarization

Figure 5 shows the probability of channel opening P_o as a function of depolarization for $T=0\,°C$ and 14 °C. For comparison, the open probability of the batrachotoxin-modified Na^+ channels at these temperatures, as measured by Correa, Bezanilla, and Latorre [17], are also reproduced. To facilitate

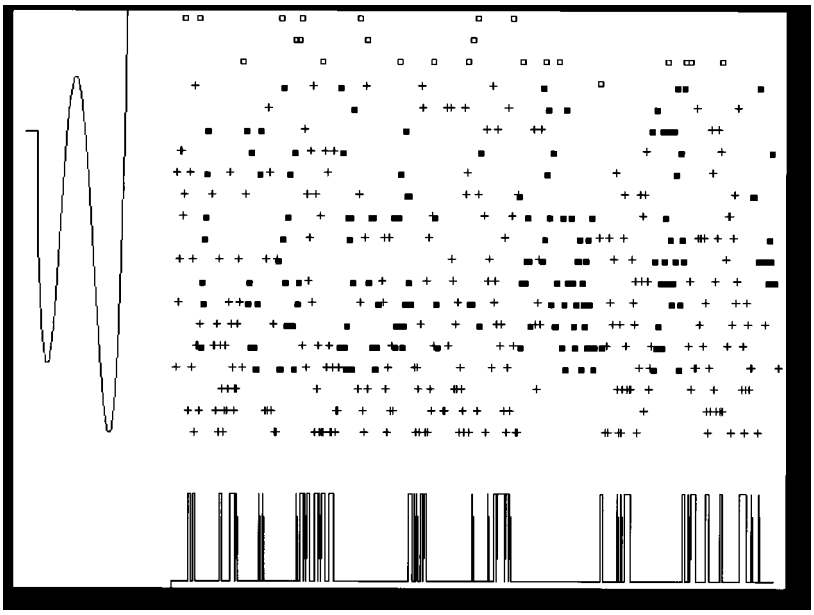

FIG. 3. Left-hand margin: double-well potential $U_{\text{tot}}(z)$ for $c=4.5$ Å and an effective electric field of 0.0155 V/Å. The depth of the right-hand well is 47.6 meV and the left-hand well has a depth of 34.7 meV. The somewhat deeper right-hand well indicates that the channel is moderately depolarized. *Upper right*: energy level of the $S4$ helix versus time for 500 successive time intervals. Each + symbol indicates a time interval in which the helix is in the activated state (right-hand well in the double-well potential at the left); filled squares indicate time intervals spent in the nonactivated state (left-hand well) and open squares correspond to intervals in the fluctuating state (above the barrier). *Lower record*: channel conductance versus time for a model channel constructed from combining four such $S4$ segment histories. The channel was considered open for time intervals during which any three of the four segments were in the activated state. Upward deflection indicates times when the channel is open, as in typical ''patch clamp'' records.

comparison, we have interpreted E_{eff} in terms of the membrane potential difference using Eq. (5). (Variations in E_{eff} of 0.0015 V/Å correspond to membrane potential changes of order 30 mV. Using this scale, we have set to zero the horizontal axis of our theoretical graph for P_o in order to compare our model with the experimental graph of Correa, Bezanilla, and Latorre [17]. Doing this is equivalent to setting a value for the F_{bal} term in E_{eff} [Eq. (4)].)

As Fig. 5 shows, the sliding helix model correctly reproduces the general features of the experimental P_o curve, including the correct horizontal shift of order 60 mV for the probability rising from 0 to near 1. It does not reproduce, however, the observed temperature dependence, i.e., the shift in P_o to the right by about 20 mV when temperature is increased by 14 °C. In the next sub-section we discuss possible adjustments to the model that might correct this lack of temperature sensitivity.

C. Open and closed times

In setting up the model, no attempt was made to tie the computational step cycle to real time. Initial calculations produced sets of open and closed times measured in units of computational step cycles, which were then associated with times based on data from batrachotoxin-modified channels [17]. Good correspondence between model output and data on channels was obtained when the computational step cycle was made equal to 10 μs (Fig. 6). The implications of this time scale for the model are considered in Sec. VI.

Figure 6 shows the mean open and closed times of the channel as a functions of depolarization and compares the calculated times, based on a computational time step of 10 μs, with those of Correa, Bezanilla, and Latorre [17]. Both the experimental data and model calculations display comparable shifts in open and closed times for depolarization of about 40 mV. The absence of any significant model temperature dependence is clearly seen in a comparison of Fig. 6(a) (0 °C) with Fig. 6(b) (14 °C).

Histograms of simulated open and closed dwell times for the channel are shown for two membrane polarizations at 0 °C in Fig. 7. Again, the comparison is with the data of Correa, Bezanilla, and Latorre [17], taken from Fig. 4 of their paper. As the figures show, both the model and simulated histograms range over three orders of magnitude in the time interval. The peak in the open time data of Correa, Bezanilla, and Latorre [17] undergoes a shift of about one log(time) unit (from -2.5 to -1.5) for depolarization of about 30 mV. The open time histograms constructed from the simulation show comparable development with depolarization. The model and experimental closed time histograms likewise show good qualitative agreement: both show the development of a second peak at longer time intervals with increasing polarization.

V. EFFECTS OF SITE SPECIFIC MUTATIONS

The preliminary nature of the model and its uncertainty in regard to such parameters as F_{bal} make it unrealistic to attempt exact predictions of the effects of changes in specific amino acids in the channel molecule. However, the physical structure of the model does allow several qualitative observations. First, replacing the positive residue at the extracellular boundary of the membrane [indexed by $p=0$ in Eq. (2)] with a neutral residue should cause the $S4$ segment to

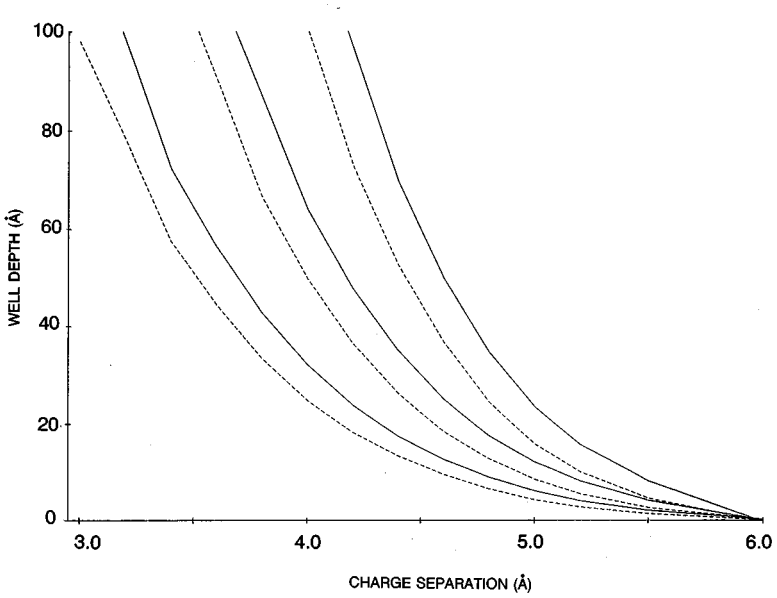

FIG. 4. Depth of potential wells of $U_{tot}(z)$, vs charge separation c, at values of effective field for which the wells are of equal depth [e.g., approximately as in Fig. 2(b)]. Three pairs of curves are shown, with the left-hand pair calculated for dielectric constant $\epsilon_r = 20$, the middle pair for $\epsilon_r = 10$, and the right-hand pair for $\epsilon_r = 5$. In each pair of curves, the solid line represents the calculation assuming six negative charges on adjacent segments. The dashed curves show the results of calculations made assuming five negative charges, with the third negative charge from the intracellular side having been removed. As can be seen from the graphs, well depths of 25–50 meV in the model are produced by charge separations between 3.5 and 5 Å.

activate at more negative membrane potentials, i.e., at less depolarized levels. This is because neutralizing a positive residue on the extracellular end of the $S4$ segment will make the Coulombic interaction energies of the shifted (i.e., activated) and unshifted (nonactivated) positions nearly equal, under the model assumption of six negative charges on surrounding segments. (Both positions will have five paired residues and one unpaired negative residue.) The wild type $S4$ segment, on the other hand, has six paired residues in its unshifted position but only five paired residues (with a net transfer of one positive charge across the membrane) in its shifted position. Thus, for the wild type $S4$, the potential well for the shifted position lies above the unshifted well in energy; however, the mutated ($p=0$) $S4$ has shifted and unshifted potential wells whose minima are equal in energy. As membrane depolarization increases, the transition statistics for activation will favor the mutated $S4$ in comparison with the wild type segment. The electric force on the helix due to E_{ext} does increase upon mutation (from $6QE_{ext}$ to $5QE_{ext}$ in magnitude), but in our computations this countering change in force is always exceeded by the change in the Coulombic binding just outlined (data not shown).

In contrast, replacing the positive residue at the cytoplasmic boundary [indexed by $p=5$ in Eq. (2)] with a neutral residue will require *less* negative potentials, i.e., larger depolarization, to cause activation. This is because the change in the Coulombic binding energy due to an outward shift will be greater for the mutated $S4$ segment in comparison with the wild type segment. It is easy to see that an asymmetry arises since the shift is always toward the extracellular boundary of the membrane. Thus our model predicts an asymmetry in the shift in depolarization needed to activate the channel, with the shift direction dependent on whether the neutralized amino acid is closer to the extracellular or cytoplasmic side of the membrane. These predictions agree with the trends in the effects of site-specific changes on the voltage for half-maximal activation reported by Stühmer *et al.* [18].

VI. DISCUSSION

A. Overview

The goal of this research has been to investigate whether the sliding helix model of sodium channel activation is physically realistic. Our approach has necessarily been tentative given the uncertainty in the molecular geometry of the channel, yet even so the results provide a broad check on the tenability of the sliding helix picture of gating. The results outlined in Figs. 5–7 show that the sliding helix model is capable of representing experimental data on several physiological characteristics of the channel. In particular, the model dependence of open probability on depolarization is in good agreement with experiment. Also, the distributions of channel open and closed dwell times at $T=0$ °C (Fig. 7) are rendered by the model with reasonable fidelity over three orders of magnitude in time. However, the absence of any significant temperature dependence in the model is especially noticeable when highlighted against these successes.

B. Time scale

The model time step is a parameter fixed by fitting the model mean open times (measured in time steps) with data on mean open times of batrachotoxin-modified sodium channels; the best fit occurred for a model time step of 10 μs. This value is many orders of magnitude longer than the time scale expected for quantum transitions between states of a simple one-dimensional harmonic oscillator: elementary

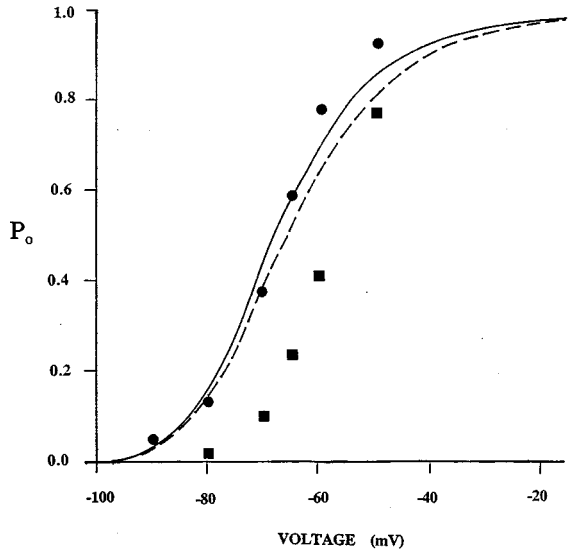

FIG. 5. Open probability P_o as a function of membrane depolarization V. A full line represents the model results for $T=0$ °C, a broken line gives the model results for $T=14$ °C. The experimental comparison is with the results of Correa, Bezanilla, and Latorre [17], as given in their Fig. 3(a). Experimental data for 0 °C are denoted using ●; date for 14.3 °C are graphed using ■. The expression of E_{eff} in terms of membrane depolarization uses the following values for model parameters: $F_{\text{bal}}=1.19\times10^{-10}$ N and $E_{\text{rest}}=2.67$ mV/Å (see Sec. VI).

quantum mechanics predicts a time scale for interstate transitions of order $\tau=1/\omega_0=10^{-12}$ s, using $\hbar\omega=0.44$ meV from the model [19]. Though this difference cannot be quantitatively accounted for within the present model, it is useful in this context to remember that a one-dimensional harmonic oscillator, uncoupled from other modes of the helix (both mechanical and electronic), is a gross simplification. It should not be surprising that actual channel transition times differ from those of an isolated harmonic oscillator. The energy of an α helix can be partitioned in many ways: electronic states of the residues, motions in the sidechains, torsional motions of the α helix, or c.m. motion. It is reasonable to suppose that coupling to these other modes affects the c.m. oscillation transition times.

C. Temperature dependence

Temperature enters the model in a simple way: E, the mean c.m. kinetic energy of the α helix, is assumed to be equal to kT (with T in K). We assume that the helix's c.m. motion is describable in terms of a simple harmonic oscillator in thermal equilibrium with its surroundings and treat the surrounding membrane as a thermal reservoir of temperature T. While such an assumption is justifiable as a starting point, it almost certainly fails to represent the complexity of the energy-exchange process between the helix and its surroundings. For example, as temperature varies, other energy modes of the α helix would be expected to come in and out of play: local electronic excitations, local vibrational modes of the helix along its axis, and torsional modes of the helix, among others. These additional energy modes, the result of the α helix's internal structure, will result in a temperature-dependent density of states for the α helix. Unfortunately, incorporation of these more complex processes would be expected to make the helix's c.m. kinetic energy less rather than more responsive to temperature changes. (That this is the case can be seen through an elementary energy partitioning argument.) Thus the present model will require other modifications if it is to predict the observed increase in activation with a temperature increase of order 10 °C.

The lack of temperature dependence in the model results from the fact that the probabilities of activation and nonactivation depend solely on the relative numbers of states in each category, which vary with the depth of the potential wells. In the present model, the effective potential U_{tot} does-not vary with temperature and thus there is no change in the number of activated states with increased temperature. Increasing T in the model shifts the helix's mean kinetic energy higher, which increases the transition rate between nonactivated and activated states without increasing the probability of the helix being in an activated state. Incorporating a temperature dependence in U_{tot} would increase the model's predicted temperature effects on channel statistics. Such a dependence might be achieved by including the effects of the charged residues' thermal motion. This motion would enter the present simulation in the form of random fluctuations in the positions of the positive and negative charges: the distances between charges $d_{pn}(z)$ would undergo random variations in time, with the rate and magnitude of the fluctuations depending on temperature. An analysis of how thermal fluctuations would affect the model is in progress [20].

D. The F_{bal} parameter

In setting values for F_{bal} and F_{rest} (terms in the definition of E_{eff}), we have been guided by one fact: depolarizations on the order of 10 mV cause measurable increases in the rate of channel opening. Such depolarizations, however, cannot produce the known characteristics of activation within the confines of the sliding helix model without an additional outward force on the helix [14]. An additional balancing force F_{bal} is needed to oppose the strong Coulombic binding force on the helix. F_{bal} cannot be so large that it swamps the periodicity (in **z**) and the Coulombic interaction since the periodic energy term in the effective potential must dominate if the α helix is to have distinct bound states localized along the z axis. Yet F_{bal} must be sufficiently strong to leave the α helix weakly bound and on the verge of an outward shift. This observation and Eq. (4), in conjunction with the computations of Fig. 5, allow us to set a model value for F_{bal}. If we assume that the open probability P_o is on the threshold of increasing from zero when E_{ext} is zero, the F_{bal} is determined by

$$\vec{E}^{0}_{\text{eff}}=\vec{E}_{\text{rest}}+\frac{\vec{E}_{\text{bal}}}{6Q},$$

where E^{0}_{eff} is the magnitude of the effective electric field when P_o is about to increase from zero. With charge separation $c=4.5$ Å, a resting membrane potential difference of -60 mV creates a resting potential E_{rest} of magnitude 2.67

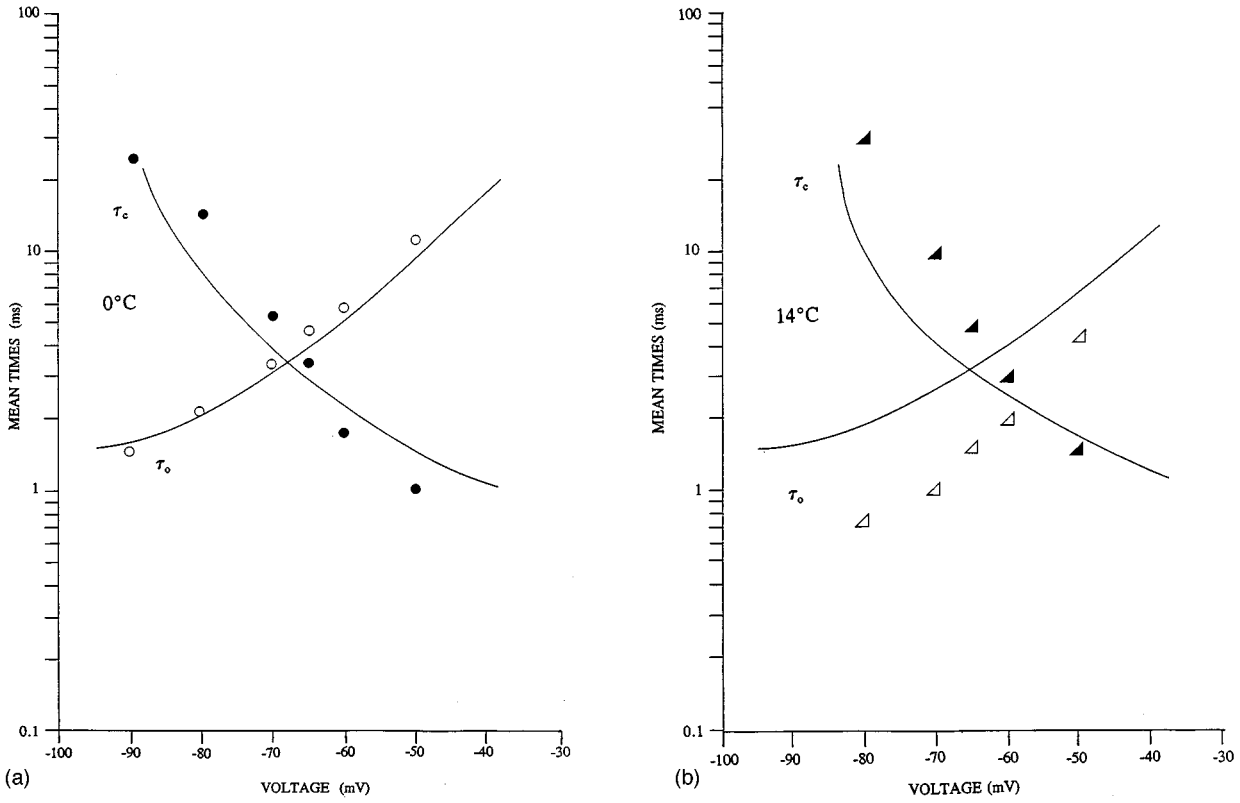

FIG. 6. Semilogarithmic plot of the mean open (τ_o) and mean closed (τ_c) times as functions of membrane depolarization for (a) $T=0$ °C and (b) $T=14$ °C. The model results (full lines) are compared against the experimental data of Correa, Bezanilla, and Latorre [17]. Open symbols show the experimental open times and filled symbols represent the experimental closed times for these two temperatures. The horizontal voltage scale for the model results was set using $F_{\text{bal}}=1.9\times10^{-10}$ N and $E_{\text{rest}}=2.67$ mV/Å (see Sec. VI). Agreement between experimental and model time intervals was achieved for a model time step of 10 μs (i.e., 500 time steps in the simulation corresponds to 5 ms).

mV/Å across the membrane, assumed to be 22.5 Å in thickness at the position of the helix [7]. The threshold value of the effective field in our simulation is 9.7 mV/Å in this case and F_{bal} then equals 1.19×10^{-10} N. We have assumed that F_{bal} is constant over helical shift distances of 0–5 Å, a reasonable starting approximation.

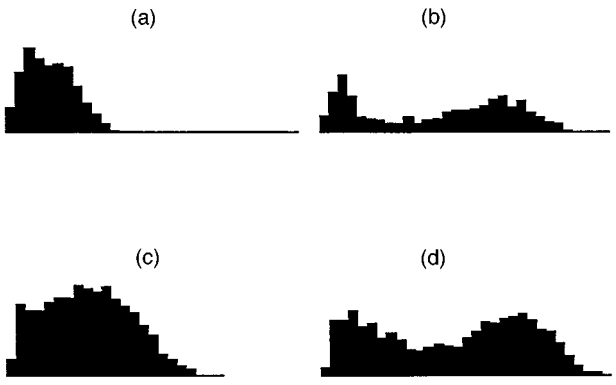

FIG. 7. Histograms of open and closed dwell times. The horizontal axis in each case indicates log(time) over 3 $\log_{10}$ units. (a) represents the open time distribution predicted by the model ($c=4.55$ Å; $E_{\text{eff}}=0.0145$ V/Å; $\epsilon_r=7$). (b) represents closed times from the same computation. (c) and (d) show measured open and closed time distributions from the data of Correa, Bezanilla, and Latorre [17] for batrachotoxin-modified Na^+ channels at -80 mV.

E. Possible inhomogeneities in the *S*4 environment

The positively charged residue nearest the exterior surface of the membrane of the *S*4 segment may become exposed to the aqueous environment after shifting outward during activation. In this situation, our treatment of the *S*4 environment as homogeneous (i.e., as having a uniform dielectric constant appropriate for peptides) would require modification. Because of its high polarizability, water will electrically shield this outermost residue, thereby reducing its Coulombic interaction with neighboring negative residues. This modification will have the general effect of promoting and maintaining outward shifts of the *S*4 helix.

F. The energy cap

The energy maximum or cap in the simulation effectively limits the c.m. kinetic energy of the *S*4 helix. It arises because the *S*4 helix is covalently bound to other portions of the channel molecule. This circumstance limits the helix's freedom of oscillation, especially at higher energies. The dis-

tribution of open and closed times is sensitive to values of the cap, especially when the cap is set close to the top of the energy barrier between the wells. However, for the computations described in this paper, the cap was set at 100 meV, which, as noted in the Introduction, is high enough that our results are not sensitive to variations in the cap. The value of 100 meV may underestimate the importance of such an effect, but we chose a conservative approach given the absence of detailed information on the channel molecule's geometry.

ACKNOWLEDGMENTS

The authors acknowledge the research assistance of Dennis Ruhl of Purdue University Calumet and Haitao Huang of Amherst College.

[1] D. Junge, *Nerve and Muscle Excitation*, 3rd ed. (Sinauer Associates, Sunderland, MA, 1992).
[2] B. Hille, *Ionic Channels of Excitable Membranes*, 2nd ed. (Sinauer Associates, Sunderland, MA, 1992).
[3] A. L. Hodgkin and A. F. Huxley, J. Physiol. London **116**, 449 (1952).
[4] B. F. Ball and J. A. Rice, Math. Biosci. **112**, 189 (1992).
[5] H. R. Guy and P. Seetharamulu, Proc. Natl. Acad. Sci. U.S.A. **83**, 508 (1986).
[6] W. A. Catterall, Science **242**, 50 (1988).
[7] M. Noda, S. Shimizu, T. Tanabe, T. Takai, T. Ikeda, H. Takahashi, H. Nakayama, Y. Kanaoka, N. Minamino, K. Kangawa, H. Matsuo, M. A. Raftery, T. Hirose, S. Imayama, H. Hayashida, T. Miyata, and S. Numa, Nature **312**, 121 (1984).
[8] J. G. Starkus and M. D. Rayner, Biophys. J. **60**, 1101 (1991).
[9] J. Patlak, Physiol. Rev. **71**, 1047 (1991).
[10] C. M. Armstrong and F. Bezanilla, J. Gen. Physiol. **63**, 533 (1974).
[11] R. D. Keynes and E. Rojas, J. Physiol. **255**, 157 (1976).
[12] F. Conti and W. Stühmer, Euro. Biophys. J. **17**, 53 (1989).
[13] R. D. Keynes, Proc. R. Soc. London Ser. B **249**, 107 (1992).
[14] C. C. Chancey. S. A. George, and P. J. Marshall, J. Biol. Phys. **18**, 307 (1992).
[15] D. W. Oxtoby and N. H. Nachtrieb, *Principles of Modern Chemistry* (CBS College Publishers, New York, 1990).
[16] C. Chothia, M. Levitt, and D. Richardson, J. Mol. Biol. **145**, 215 (1981).
[17] A. M. Correa, F. Bezanilla, and R. Latorre, Biophys. J. **61**, 1332 (1992).
[18] W. Stühmer, F. Conti, H. Suzuki, X. Wang, M. Noda, N. Yahagi, H. Kubo, and S. Numa, Nature **339**, 597 (1989).
[19] C. V. Heer, *Statistical Mechanics, Kinetic Theory, and Stochastic Processes* (Academic, New York, 1972).
[20] C. C. Chancey, S. A. George, H.-T. Huang, and D. Ruhl (unpublished).